Employing Whole-Body Control in Assistive Robotics

Maged Iskandar, Gabriel Quere, Annette Hagengruber, Alexander Dietrich, and Jörn Vogel

***Abstract*— Light-weight robotic manipulators in combination with power wheelchairs can help to restore the mobility of people with disabilities. While such systems are available on the market, they typically are limited to fully manual control modes. In research, shared control methods are employed, to increase the usability of these systems. Here, we present an additional extension, by introducing a whole-body control concept to the assistive robotic system EDAN. Combined with shared control, the whole-body controller allows the realization of complex tasks which necessitate the coordination of arm and platform, while ensuring compliant behavior resulting from the impedance control law. The implemented approach is analyzed and validated in an exemplary task of opening a door, passing through it and closing it afterwards. While this task would exceed the reachability of the arm in a classical approach, the combination of whole-body control with a shared control scheme allows for quick and efficient execution.**

I. Introduction

Assistive devices enable people with motor disabilities to get a part of their independence back. For instance, power wheelchairs can help to restore the mobility of the individual to a large extent. However, despite the assistive device, supposed simple tasks like opening a door or pushing an elevator button, may already require the assistance of a caretaker.

Manipulation abilities, as well as reach and grasp tasks, are often huge problems for people with motor disabilities. For people with weak but remaining arm and hand function, arm support systems (passive or active) can be used to allow them to interact with their environment [1], [2]. Nowadays, robotic manipulators for people without remaining arm and/or hand function are becoming more available [3]. Initially, such systems were meant as stationary robots, which were designed for highly specific tasks such as turning the pages of a book, or feeding [4], [5]. In combination with a power wheelchair, such manipulation aids could help to restore the mobility of affected people to a large extent. Research on wheelchair-mounted robotic manipulators has started in the late 1970s already [6]; the first commercially available system was the MANUS manipulator released in the 1990s [7]. Nowadays, there are a few wheelchair-mountable robotic manipulators available, e.g. the MANUS successor iARM [8], or the JACO arm [3].

However, from a robotic perspective, the usability of these systems can still be largely increased. At the German Aerospace Center (DLR), we are developing an assistive robotic system called EDAN [9], which serves as a development platform for different aspects of rehabilitation robotics. For one, this is comprised of research on interfaces to provide people with severe motor-disability with control over such systems [10], [11]. Additionally, we are also developing shared-control methods to guide the end-effector based on the user commands, to improve the usability of such robotic systems [12]. The goal of this paper is to develop whole-body control for the EDAN system, which is combined with a shared control scheme to provide an efficient user-centered method in order to accomplish tasks that require a large range of motion. However, this requires continuous coordination between the platform and the arm motions. Typical examples of this could be fixing the absolute position of the robot hand while performing motion with the wheelchair or trying to open and pass through a door, a task in which arm and wheelchair have to be moved at the same time, in order to perform it efficiently.

Fig. 1: The assistive robotic system EDAN (EMG-controlled daily assistant).

The coordination between the robotic manipulator and the mobile base is a classical problem in robotics [13], [14]. As the underlying control methods are generally known [15], [16], we focus on the application to the assistive robotics system while a new actuation concept for the mobile base is developed to create a system behavior that is transparent to the user. Door opening with a mobile manipulator has already been extensively studied in the literature, with various approaches, usually focused on control [17], but also on path planning [18]. However, we are among the first to employ and experimentally validate such a whole-body motion strategy combined with shared control to achieve assistive tasks.

All authors are with the Institute of Robotics and Mechatronics, German Aerospace Center (DLR), Wessling, Germany. Email: maged.iskandar@dlr.de. This work is partly supported by the Bavarian Ministry of Economic Affairs, Regional Development and Energy, within the project "SMiLE" (LABAY97) and "SMiLE2gether", (LABAY102).

II. Background

A. System Description

The robotic wheelchair EDAN (EMG-controlled daily assistant) is a fully integrated wheelchair-based manipulation aid for people with severe motor impairment. EDAN is composed of a state-of-the-art power wheelchair and a torque-controlled robotic arm mounted on the right side of the wheelchair, see Fig. 1. The mobile base of EDAN, an F5-Corpus VS of the company Permobil, is a commercially available wheelchair designed for people with severe physical disabilities. It provides a front-wheel drive and pivot-rear-wheels. As the wheelchair does not provide an odometry model or wheel encoders, we equipped each front-wheel with a magnetic ring encoder to precisely measure the wheels rotations ϕ_1 and ϕ_2. For manipulation, a DLR Light-Weight Robot III (LWR3) is used, which is enhanced with an additional (8th) axis at the arms-base, to be able to reach to the ground. The arm is equipped with a dexterous torque-controlled five-fingered DLR-HIT hand for grasping and manipulation. To control the motion of the system, i.e. move the arm or the wheelchair, a 3D-velocity command is used. Currently, the system can be interfaced either by a conventional joystick or alternatively by an interface based on electromyography (EMG). This EMG-based interface allows people to operate robotic systems continuously in 3D, when the use of a joystick is not an option due to the users impairment [19].
Furthermore, the system is equipped with an Asus Xtion Pro Live RGB-D camera to perceive the environment as well as an integrated head switch for additional user input. All hardware, including the computers, is mounted on the wheelchair such that the system can be self-sufficient.

B. Shared Control

EDAN provides a manual control mode, in which the user is permanently in control over translations and rotations and can use the head-switch to change between manipulator and wheelchair control. Additionally, EDAN provides a shared control mode to support the user during specific tasks. Supposedly *easy* tasks like drinking or opening a door consist of many different subtasks like grasping, positioning or performing defined rotations, all of which require precise control of the robotic arm. Shared control algorithms can help to interact more efficiently with the environment by using task specific symbolic and geometric information.

In the case of EDAN, the RGB-D camera is used to detect and localize known objects, from which the shared control module can infer tasks. The shared control functionality is applied in terms of virtual fixtures, e.g. if the user moves the end-effector in the direction of an object (for a specific task), the shared control algorithm will guide the end-effector accordingly. A task is defined as a state machine with multiple states and transitions; states define position constraints on the end-effector and the mapping for the guided commands. A more detailed description of the shared control approach implemented on EDAN is beyond the scope of this paper, as the focus of this work is the whole-body control, presented below.

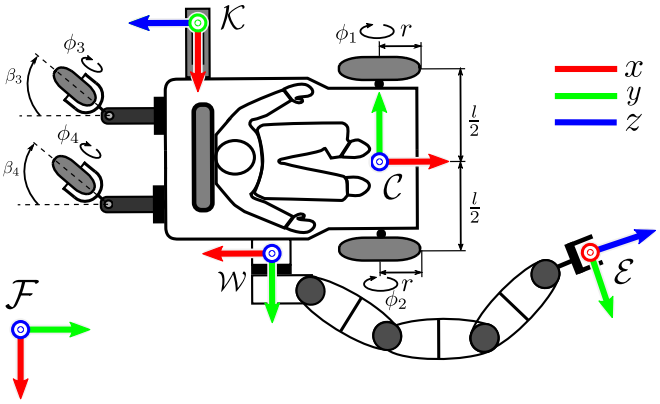

Fig. 2: Schematic representation of the EDAN system illustrating the different coordinate systems and variables.

C. Dynamic Formulation

A wheelchair-based manipulation aid such as EDAN presents a sophisticated robotic system with multiple degrees of freedom (DOF). Such a system as shown in Fig. 2 can be described by the dynamic equations of motion through

$$\boldsymbol{M}(\boldsymbol{y})\ddot{\boldsymbol{y}} + \boldsymbol{C}(\boldsymbol{y},\dot{\boldsymbol{y}})\dot{\boldsymbol{y}} + \boldsymbol{g}(\boldsymbol{y}) = \boldsymbol{H}\boldsymbol{\tau} + \boldsymbol{\tau}^{\text{ext}} + \boldsymbol{A}(\boldsymbol{y})^T\boldsymbol{\lambda} \tag{1}$$

$$\boldsymbol{A}(\boldsymbol{y})\dot{\boldsymbol{y}} = \boldsymbol{0} \tag{2}$$

where the configuration is described by

$$\boldsymbol{y} = \begin{pmatrix} \boldsymbol{q}_b \\ \boldsymbol{q}_m \end{pmatrix} \tag{3}$$

with the configuration $\boldsymbol{q}_b \in \mathbb{R}^9$ of the mobile base and the manipulator configuration $\boldsymbol{q}_m \in \mathbb{R}^8$. The gravitational effects are represented by $\boldsymbol{g}(\boldsymbol{y}) \in \mathbb{R}^{17}$, and the inertia and Coriolis/centrifugal matrices are defined by $\boldsymbol{M}(\boldsymbol{y}), \boldsymbol{C}(\boldsymbol{y},\dot{\boldsymbol{y}}) \in \mathbb{R}^{17\times 17}$, respectively. The configuration coordinates of the mobile platform can be defined as

$$\boldsymbol{q}_b = \begin{bmatrix} \boldsymbol{\xi} \\ \boldsymbol{\beta} \\ \boldsymbol{\phi} \end{bmatrix}, \tag{4}$$

with the posture coordinates $\boldsymbol{\xi} = [x_{\mathcal{C}}\ y_{\mathcal{C}}\ \theta_{\mathcal{C}}]^T$ defined in frame $\mathcal{C}$ w. r. t. the frame $\mathcal{F}$ as in Fig. 2, the orientation coordinates of the off-centered rear-wheels (caster wheels) $\boldsymbol{\beta} = [\beta_3\ \beta_4]^T$, and the rotational coordinates of the fixed and the caster wheels $\boldsymbol{\phi} = [\phi_1\ \phi_2\ \phi_3\ \phi_4]^T$. Let $\boldsymbol{\tau} \in \mathbb{R}^{10}$ be the actuation forces and $\boldsymbol{H} \in \mathbb{R}^{17\times 10}$ describe the mapping from actuation forces to generalized forces acting collocated to $\dot{\boldsymbol{y}}$. Additionally, $\boldsymbol{\tau}^{\text{ext}} \in \mathbb{R}^{17}$ are the external forces and $\boldsymbol{A}(\boldsymbol{y}) \in \mathbb{R}^{2\times 17}$ is the constraint Jacobian matrix that is imposed by the non-integrable constraints (nonholonomic) of the fixed wheels. The end-effector twist is given by

$$\dot{\boldsymbol{x}} = \begin{pmatrix} \boldsymbol{J}_b & \boldsymbol{J}_m \end{pmatrix} \dot{\boldsymbol{y}} \tag{5}$$

with the respective Jacobian matrices $\boldsymbol{J}_b \in \mathbb{R}^{6\times 9}$ and $\boldsymbol{J}_m \in \mathbb{R}^{6\times 8}$, formulating the whole-body Jacobian matrix

of the mobile robot. In addition, $\boldsymbol{\lambda} \in \mathbb{R}^2$ is the Lagrangian multiplier which limits the unfeasible directions of motion.

D. Mobile Platform Modeling and Control Interface

The state-space configuration kinematic model of the mobile platform (wheelchair) of EDAN subjected to independent velocity constraints can be written in the form

$$\dot{\boldsymbol{q}}_b = \underbrace{\begin{bmatrix} \boldsymbol{R}(\theta_{\mathcal{C}})^T \boldsymbol{\Sigma} \\ \boldsymbol{B}(\boldsymbol{\beta})\boldsymbol{\Sigma} \\ \boldsymbol{E}(\boldsymbol{\beta})\boldsymbol{\Sigma} \end{bmatrix}}_{\boldsymbol{s}(\boldsymbol{q}_b)} \underbrace{\begin{bmatrix} r/2 & r/2 \\ r/l & -r/l \end{bmatrix} \begin{bmatrix} \dot{\phi}_1 \\ \dot{\phi}_2 \end{bmatrix}}_{\boldsymbol{\eta}} . \tag{6}$$

The vector $\boldsymbol{\eta}$ represents the generalized body velocities which, in case of a differential-drive platform, are the heading direction (forward) and the angular velocity, respectively. Additionally, r is the radius of the front wheels and l is the distance between the centers of these, as shown in Fig. 2. The dimension of the velocity vector can also be seen as the degree of mobility of the mobile platform $\sigma_m = 2$. As depicted in Fig. 2, no steering wheels are present on the system, hence, the degree of steerability is $\sigma_s = 0$, resulting in a type (2,0) categorization [20]. In addition the two passive caster wheels do not provide an additional velocity constraint on the platform motion. The platform does not have actively orientable wheels, therefore matrix $\boldsymbol{\Sigma} \in \mathbb{R}^{3\times 2}$ is constant and it represents the null space of the fixed wheels constraints [20], such that for all times there exists a time-varying vector $\boldsymbol{\eta}(t)$ where (6) is valid. Here, $\boldsymbol{R}(\theta_{\mathcal{C}})$ is the rotation matrix calculated from the angle $\theta_{\mathcal{C}}$. The term $\boldsymbol{B}(\boldsymbol{\beta})$ represents the side-way slipping constraints of the caster wheels and $\boldsymbol{E}(\boldsymbol{\beta})$ stands for the rolling constraints for the four wheels. For more details on $\boldsymbol{E}(\boldsymbol{\beta})$ and $\boldsymbol{B}(\boldsymbol{\beta})$, the reader is referred to [20] and [21]. This is a full-state kinematic model and it can be simplified to keep only the posture coordinates $\boldsymbol{\xi}$ by using the subset which is relevant to the fixed differential wheels. In general, we are interested in keeping track of the estimated caster wheel orientations $\boldsymbol{\beta}$, as they can be used as an additional predictor for the path that the user is commanding, but this is beyond the scope of this paper. The end-effector twist can be written as

$$\dot{\boldsymbol{x}} = \mathrm{Ad}_{g_{\mathcal{C}\mathcal{E}}^{-1}} \boldsymbol{\nu}_b + \boldsymbol{J}_m \dot{\boldsymbol{q}}_m \tag{7}$$

where $\mathrm{Ad}_{g_{\mathcal{C}\mathcal{E}}^{-1}}$ is the adjoint of the transformation from frame $\mathcal{E}$ to $\mathcal{C}$. Furthermore, the base velocity $\boldsymbol{\nu}_b$ can be obtained from the velocity vector $\dot{\boldsymbol{\xi}}$ in a straightforward fashion. Now the contribution of the base velocity has been included.

E. Mobile Platform Velocity Control

Since the platform of EDAN is a commercially available power-wheelchair, commanding the platform is restricted to the functionalities provided by the proprietary interface. This interface allows for commanding of analog signals corresponding to the forward and the angular velocities of the wheelchair in an open loop manner. Correspondingly, these velocities are the DOF that can be manipulated in relation to $\boldsymbol{\eta}$ as it corresponds to the instantaneous mobility of a mobile platform of type (2,0), see [21]. Thus, $\boldsymbol{\eta}$ is separately controlled as a subsystem to be able to command arbitrary desired velocities. The controller objective is to minimize the velocity error $\tilde{\boldsymbol{\eta}} = \boldsymbol{\eta} - \boldsymbol{\eta}_{\mathrm{d}}$ where $\boldsymbol{\eta}_{\mathrm{d}}$ represents the desired velocity vector. A proportional-integral (PI) controller and a velocity feed-forward term are employed to achieve the desired behavior. However, evaluation of the control performance revealed that constant controller gains are not sufficient for covering the operating velocity range of the wheelchair. Therefore, the controller gains are adjusted automatically with respect to the velocity by utilizing a gain scheduling approach as

$$\boldsymbol{u} = \boldsymbol{\eta}_{\mathrm{d}} - \boldsymbol{K}_{p\eta}(\boldsymbol{\eta})\tilde{\boldsymbol{\eta}} - \boldsymbol{K}_{I\eta}(\boldsymbol{\eta}) \int \tilde{\boldsymbol{\eta}}\, dt \ , \tag{8}$$

where $\boldsymbol{u}$ is the control action assigned to the wheelchair. The minimum and maximum operating velocity points are selected to be the two design points for the gain scheduling method. Additionally, the scheduling of the controller gains $\boldsymbol{K}_{p\eta}(\boldsymbol{\eta})$ and $\boldsymbol{K}_{I\eta}(\boldsymbol{\eta})$ is assumed to be linear w. r. t. the velocity. By applying this control structure a good tracking performance is achieved, see Section IV-B.

F. Admittance Interface to the Mobile Platform

The shaping of the original platform dynamics can be achieved directly using the above-described velocity controller together with an admittance interface [15]. In this way the desired forces and torques can be transformed to the required velocities and applied to the mobile platform.

$$\boldsymbol{M}_{adm}\dot{\boldsymbol{\eta}}_{\mathrm{d}} + \boldsymbol{D}_{adm}\boldsymbol{\eta}_{\mathrm{d}} = \boldsymbol{\tau}_b + \boldsymbol{\tau}_b^{\mathrm{ext}} \ . \tag{9}$$

The desired mobile base dynamics is parameterized by $\boldsymbol{M}_{adm}, \boldsymbol{D}_{adm}$ which are the virtual platform inertia and damping of the admittance interface, respectively. The mobile platform force/torque $\boldsymbol{\tau}_b$ can be used as the admittance control input. Note that the generalized external forces $\boldsymbol{\tau}_b^{\mathrm{ext}}$ acting on the platform can be used to realize a whole-body impedance causality.

G. Overall Dynamics (in Reduced Form)

The standard method to write the unconstrained dynamics and reduce the dimension of the system equations[1] is to apply a coordinate transformation as

$$\dot{\boldsymbol{y}} = \underbrace{\begin{bmatrix} \boldsymbol{s} & 0 \\ 0 & \boldsymbol{I} \end{bmatrix}}_{\boldsymbol{S}} \begin{bmatrix} \boldsymbol{\eta} \\ \dot{\boldsymbol{q}}_m \end{bmatrix} \ . \tag{10}$$

Using the property $\boldsymbol{S}\boldsymbol{A} = \boldsymbol{0}$, the nonholonomic constraints imposed from the platform can be eliminated such that (2) can be straightforwardly transformed to the unconstrained dynamics

$$\bar{\boldsymbol{M}} \begin{bmatrix} \dot{\boldsymbol{\eta}} \\ \ddot{\boldsymbol{q}}_m \end{bmatrix} + \bar{\boldsymbol{C}} \begin{bmatrix} \boldsymbol{\eta} \\ \dot{\boldsymbol{q}}_m \end{bmatrix} + \bar{\boldsymbol{g}} = \begin{bmatrix} \boldsymbol{\tau}_b \\ \boldsymbol{\tau}_m \end{bmatrix} + \begin{bmatrix} \boldsymbol{\tau}_b^{\mathrm{ext}} \\ \boldsymbol{\tau}_m^{\mathrm{ext}} \end{bmatrix}, \tag{11}$$

[1]Note that dependencies on the states have been omitted for the sake of readability.

with

$$\bar{\boldsymbol{M}} = \boldsymbol{S}^T \boldsymbol{M} \boldsymbol{S} \tag{12}$$

$$\bar{\boldsymbol{C}} = \boldsymbol{S}^T \left(\boldsymbol{M} \dot{\boldsymbol{S}} + \boldsymbol{C} \boldsymbol{S} \right) \tag{13}$$

$$\bar{\boldsymbol{g}} = \boldsymbol{S}^T \boldsymbol{g} \ . \tag{14}$$

Moreover, the force-torque command $\boldsymbol{\tau}_b$ through the admittance (9) can be directly used to control the velocities which are instantaneously feasible w. r. t. the nonholonomic constraints. By means of the kinematic relation (8) to control the mobile platform and under the assumption of an ideal kinematic controller $\boldsymbol{\eta} \approx \boldsymbol{\eta}_d$, the dynamics can be shaped [16] by the parameters of the admittance interface as

$$\bar{\boldsymbol{M}} = \begin{bmatrix} \boldsymbol{M}_{\text{adm}} & \boldsymbol{0} \\ \boldsymbol{M}_{m,\eta} & \boldsymbol{M}_{m,m} \end{bmatrix} \tag{15}$$

$$\bar{\boldsymbol{C}} = \begin{bmatrix} \boldsymbol{D}_{\text{adm}} & \boldsymbol{0} \\ \boldsymbol{C}_{m,\eta} & \boldsymbol{C}_{m,m} \end{bmatrix} \tag{16}$$

$$\bar{\boldsymbol{g}} = \begin{bmatrix} \boldsymbol{0} \\ \boldsymbol{g}_m \end{bmatrix}. \tag{17}$$

The quantities $\bar{\boldsymbol{M}}, \bar{\boldsymbol{C}} \in \mathbb{R}^{(10\times 10)}$ denote the whole-body inertia and Coriolis/centrifugal matrices, respectively, and $\bar{\boldsymbol{g}} \in \mathbb{R}^{10}$ represents the gravitational terms. The actuation force/torque for the mobile base and manipulator are $\boldsymbol{\tau}_b \in \mathbb{R}^2$ and $\boldsymbol{\tau}_m \in \mathbb{R}^8$, respectively. For simplicity the friction torques are omitted in (11), in practice they can be compensated for using a model or observer based approach [22]–[24].

III. Methodology and Control Design

Keeping the system behavior transparent to the user is the main concern while developing the control algorithm. Therefore a new actuation method is developed for the mobile platform (wheelchair) to perform motion in a predictable way. In addition, the dynamics formulation (11) allows to implement different control modes.

A. Whole-Body Control Mode (WBC)

The objective here is to apply a whole-body coordination control in order to perform tasks that require a large range of motion, such as opening or closing a door. If a compliant behavior at the end-effector is required, hierarchical impedance control can be employed. The joint control torques in the manipulator can be expressed as

$$\boldsymbol{\tau}_m = \boldsymbol{\tau}_{\text{imp}} + \boldsymbol{\tau}_{\text{null}} + \boldsymbol{g}_m, \tag{18}$$

where $\boldsymbol{\tau}_{\text{imp}}$ realizes the Cartesian impedance at the end-effector [24], the term $\boldsymbol{\tau}_{\text{null}}$ achieves a null space task, and $\boldsymbol{g}_m$ stands for the active (model-based) gravity compensation. The classical structure of the Cartesian regulation control can be formulated as

$$\boldsymbol{\tau}_{\text{imp}} = -\boldsymbol{J}_m^T (\boldsymbol{K} \tilde{\boldsymbol{x}} + \boldsymbol{D} \dot{\boldsymbol{x}}), \tag{19}$$

with the task-space error $\tilde{\boldsymbol{x}} = \boldsymbol{x} - \boldsymbol{x}_d$ defining the deviation between the actual Cartesian coordinates $\boldsymbol{x}$ and the desired ones $\boldsymbol{x}_d$ of the robot arm. The Cartesian stiffness and damping matrices are represented by $\boldsymbol{K}, \boldsymbol{D} \in \mathbb{R}^{6\times 6}$. The control

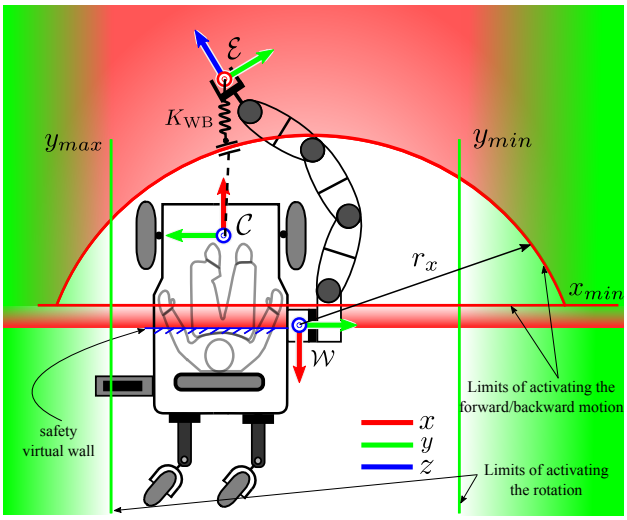

Fig. 3: Virtual boundaries of the whole-body control (WBC) in x-y plane. The WBC builds up potential from K_{WB} when the robot hand exceeds the maximum or minimum limits on x and y, and applies it to the corresponding direction.

of the redundant DOF takes place in the statically consistent null space of the Jacobian matrix $\boldsymbol{J}_m$ of the main task [25]. Furthermore, the regulation control of the elbow position is implemented to provide a more compact configuration (width) of the system, for example to fit through a door. The control action related to the null space task is

$$\boldsymbol{\tau}_{\text{null}} = -\boldsymbol{N} \boldsymbol{J}_{\text{elbow}}^T \boldsymbol{f}_{\text{elbow}} \tag{20}$$

where the corresponding null space projector is denoted by $\boldsymbol{N} \in \mathbb{R}^{8\times 8}$ while $\boldsymbol{J}_{\text{elbow}} \in \mathbb{R}^{6\times 8}$ and $\boldsymbol{f}_{\text{elbow}} \in \mathbb{R}^6$ are the elbow Jacobian matrix and wrench, respectively. Similar to (19) the elbow wrench is calculated with a Cartesian stiffness and damping applied to the elbow frame.

The forces that are applied to the mobile base are calculated by introducing end-effector-boundaries in which the platform motion should occur. In Fig. 3 these boundaries are visualized in the x-y plane and parameterized by $[x_{min}; r_x], [y_{min}; y_{max}]$. From these parameters two nonlinear dead zone functions $h_1(x_\mathcal{E}, y_\mathcal{E})$ and $h_2(y_\mathcal{E})$ are defined in order to create the working area of the platform motion (WBC):

$$h_1(x_\mathcal{E}, y_\mathcal{E}) = \begin{cases} \sqrt{x_\mathcal{E}^2 + y_\mathcal{E}^2} - r_x & : if\ \sqrt{x_\mathcal{E}^2 + y_\mathcal{E}^2} \geq r_x \\ x_\mathcal{E} - x_{min} & : if\ x_\mathcal{E} < x_{min} \\ 0 & : else \end{cases} \tag{21}$$

and

$$h_2(y_\mathcal{E}) = \begin{cases} y_\mathcal{E} - y_{max} & : if\ y_\mathcal{E} \geq y_{max} \\ y_\mathcal{E} - y_{min} & : if\ y_\mathcal{E} < y_{min} \\ 0 & : else \end{cases} \tag{22}$$

where $x_\mathcal{E}$ and $y_\mathcal{E}$ are the end-effector x and y positions w. r. t. the manipulator base frame $\mathcal{W}$. As a result, the boundaries move with the platform, creating a transparent behavior to the user. Based on $h_1(x_\mathcal{E}, y_\mathcal{E})$ and $h_2(y_\mathcal{E})$ the commanded

platform force/torque is computed via a potential function as

$$\boldsymbol{\tau}_b = \boldsymbol{K}_{\mathrm{WB}} \begin{bmatrix} h_1(x_{\mathcal{E}}, y_{\mathcal{E}}) & 0 \\ 0 & h_2(y_{\mathcal{E}}) \end{bmatrix} \tag{23}$$

where $\boldsymbol{K}_{\mathrm{WB}} \in \mathbb{R}^{2\times 2}$ is a diagonal stiffness matrix. Using (23) the virtual spring $\boldsymbol{K}_{\mathrm{WB}}$ starts to generate command forces to the platform once the boundaries are exceeded as visualized in Fig. 3. The potential is initiated by the output of the function $h_1(x_{\mathcal{E}}, y_{\mathcal{E}})$ in the linear forward/backward directions and $h_2(y_{\mathcal{E}})$ in the rotational direction. In this case during WBC tasks the user can give velocity commands to the end-effector without caring about the wheelchair motion. Moreover, the parameters of functions (21) and (22) are usually changing on-line based on the task requirements via the shared control scheme in order to ensure reachability for the arm. Additionally, $\boldsymbol{\tau}_b$ could also be combined from different sources, for example to avoid collisions with the environment.

B. Following Mode

In some situations or tasks it can be useful to let the system follow the physical interactions at the robot hand. Essentially this means pulling and pushing on the manipulator end-effector will create a motion of the platform as a result of this interaction. To achieve this behavior, the momentum-based disturbance observer [26] is used to estimate the external joint torques $\boldsymbol{\tau}_m^{\mathrm{ext}}$ produced from the interaction with the robot arm. Here the external forces acting on the mobile platform $\boldsymbol{\tau}_b^{\mathrm{ext}}$ are neglected as they are not available by a direct measurement. The external wrench at the end-effector is directly related to the external joint torques by the Jacobian matrix $\boldsymbol{J}_m$. The end-effector external wrench is mapped to the frame at which the arm is attached to the mobile platform by

$$\boldsymbol{\tau}_b = \mathrm{Ad}^T_{g^{-1}_{\mathcal{WE}}} \boldsymbol{J}_m^{T\#} \boldsymbol{\tau}_m^{\mathrm{ext}} \,, \tag{24}$$

where $\boldsymbol{J}_m^{\#}$ is the pseudo-inverse of the manipulator Jacobian matrix[2]. Using (24) the force/torque can be applied to the platform via the admittance interface (9) to generate a velocity command. In this mode the parameters of the admittance interface play an important role in shaping the platform dynamics with respect to the force applied by the user. Now, the wheelchair can be manually maneuvered simply by interacting with the hand of the system directly without the need of an extra input device. Footage of this control mode is available in the video attachment accompanying this manuscript.

IV. Experiments

The above mentioned control algorithms have been integrated into the EDAN system to add the capability of performing whole-body tasks. In the following, the performance of the subparts of the control structure are evaluated and an exemplary application is discussed.

[2]Note that from an application point of view usually either the Whole-Body Control Mode or the Following Mode is used exclusively. As a result, $\boldsymbol{\tau}_b$ is either used from (23) or (24), accordingly.

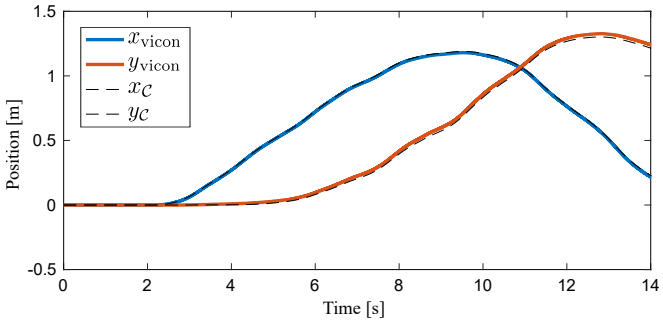

Fig. 4: Experimental validation of the odometry model. The estimated positions $x_{\mathcal{C}}$ and $y_{\mathcal{C}}$ from (4) are compared to the ground truth x_{vicon} and y_{vicon} recorded via the tracking system.

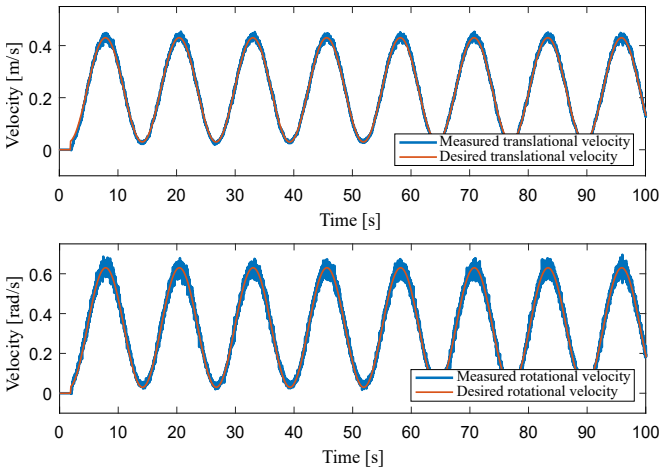

Fig. 5: The mobile platform velocity controller evaluation. The forward and angular velocity are commanded with synchronized sinusoidal signals.

A. Odometry Model Validation

The odometry model for the mobile base described in (6) is used during the whole-body motion, hence the precision of the end-effector position is highly dependent on the model quality of the odometry. To validate that model with the real behavior of the wheelchair, we used a visual tracking system from Vicon Motion Systems. The results of the experimental validation can be seen in Fig. 4. The small accumulated error (not exceeding 1cm per meter) is mostly due to slipping and uncertainty resulting from the pneumatic tires. Notably, the tracking system imposes a small validation area but as in practice the odometry is reset at the beginning of a task, the odometry precision is sufficient for the application.

B. The Mobile Platform Velocity Control

The platform velocity controller represents the base layer for the complete control structure. Therefore, experimental validation is carried out to validate the performance of the proposed velocity controller of the mobile base. A combined motion is commanded with two sinusoidal signals for the forward and the angular velocities, as depicted in Fig. 5. The classical PI controller is tuned empirically at low and high velocity, then linear gain scheduling is used with the velocity as a scheduling variable as in (8). The proposed control structure shows good tracking performance with a

root-mean-square error of 0.0071 m/s for the forward velocity and 0.0163 rad/s for the angular velocity.

C. Application: open, pass through and close a door

In the context of assistive robotics, the whole-body controller can most effectively be used in tasks requiring coordination between platform and arm motions. An illustrative example is the task of opening a door. We implemented WBC with shared control on the EDAN system to demonstrate the efficiency of our controller, see Section II-B.

The compliant end-effector behavior is kept to ensure smooth and safe interaction with the environment. This task can be split into three subtasks, namely detection of the door and alignment of the wheelchair, opening of the door and passing through it, and finally closing the door. The experimental validation is depicted in Fig. 9.

(a) Plane estimation. (b) Box detector. (c) Handle position.

Fig. 6: Pipeline for the door handle position estimation.

1) Door detection and alignment: Knowledge of the door position is needed for the automatic alignment of the wheelchair and the shared control method. To achieve this, the handle position needs to be estimated w. r. t. the camera frame $\mathcal{K}$. Therefore, the plane formed by the door is detected within the depth image Fig. 6a, and a Retinanet box detector [27], fine-tuned with 250 annotated images, is used to detect the position $\mathcal{H}_{RGB}$ of the handle in the RGB-image, see Fig. 6b. The intersection of the door plane and the vector $\overrightarrow{\mathcal{K}\mathcal{H}_{RGB}}$ computes the full handle frame $\mathcal{H}$ Fig. 6c, given that the orientation of the handle is already known w. r. t. the door. The wheelchair then aligns normal to the door with a position controller to minimize the orientation error $\tilde{\theta}$ (the orientation difference between the platform frame $\mathcal{C}$ and the handle frame $\mathcal{H}$).

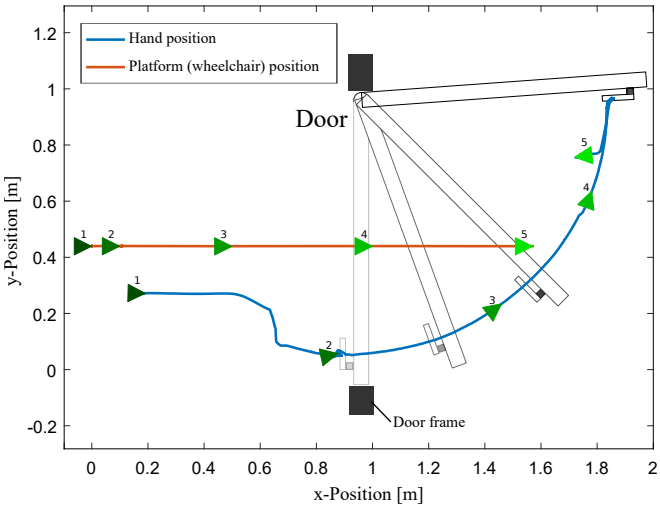

Fig. 7: Top-down view of the hand and mobile platform positions during the 'opening and passing through the door' task. The numbered arrows visualize the progress of the task in time.

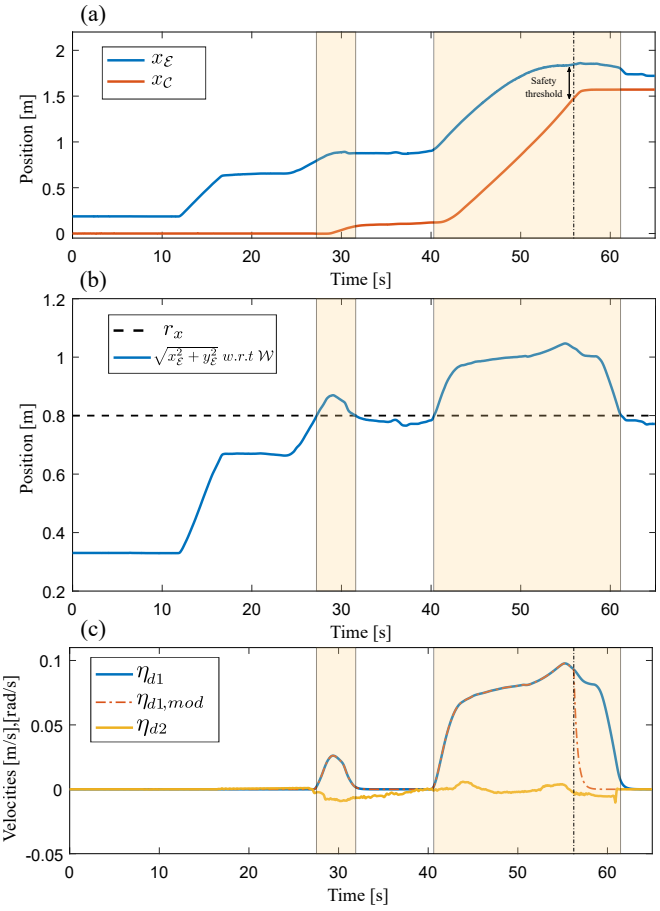

Fig. 8: Whole-body control behavior while opening the door. (a) Arm and platform motions. (b) Elongation of the virtual spring together with the forward circular boundary r_x. (c) Resulting velocity commanded to the mobile platform where η_{d1} and η_{d2} are the desired forward and angular velocity, respectively and $\eta_{d1,mod}$ is the resulting forward velocity after an additional safety check is applied.

2) Door passing: Once the mobile platform is aligned normal to the door plane, the user can open the door by providing a velocity input command to the manipulator, which is applied in combination with shared control. The first state of the shared control task guides the user towards a pre-grasp frame as shown in Fig. 9B-D; during this state, the WBC boundaries are applied and once the limit r_x =0.8 m is exceeded the spring force (23) activates. This force is transformed through the admittance interface (9) resulting in a commanded velocity applied to the platform, see Fig. 8.

The user commands the manipulator to press down the handle in the second state Fig. 9E, and then opens the door by commanding forward velocities during the third state, in which the shared control module constrains the robotic hand to stay on the path described by the handle, see Fig. 9F-J. During this state, the arm and the wheelchair motions are coordinated from the WBC, while the position of the end-effector is continuously commanded w. r. t. $\mathcal{F}$ from the shared control scheme. When going through the door, the wheelchair is limited to one DOF, allowing forward and

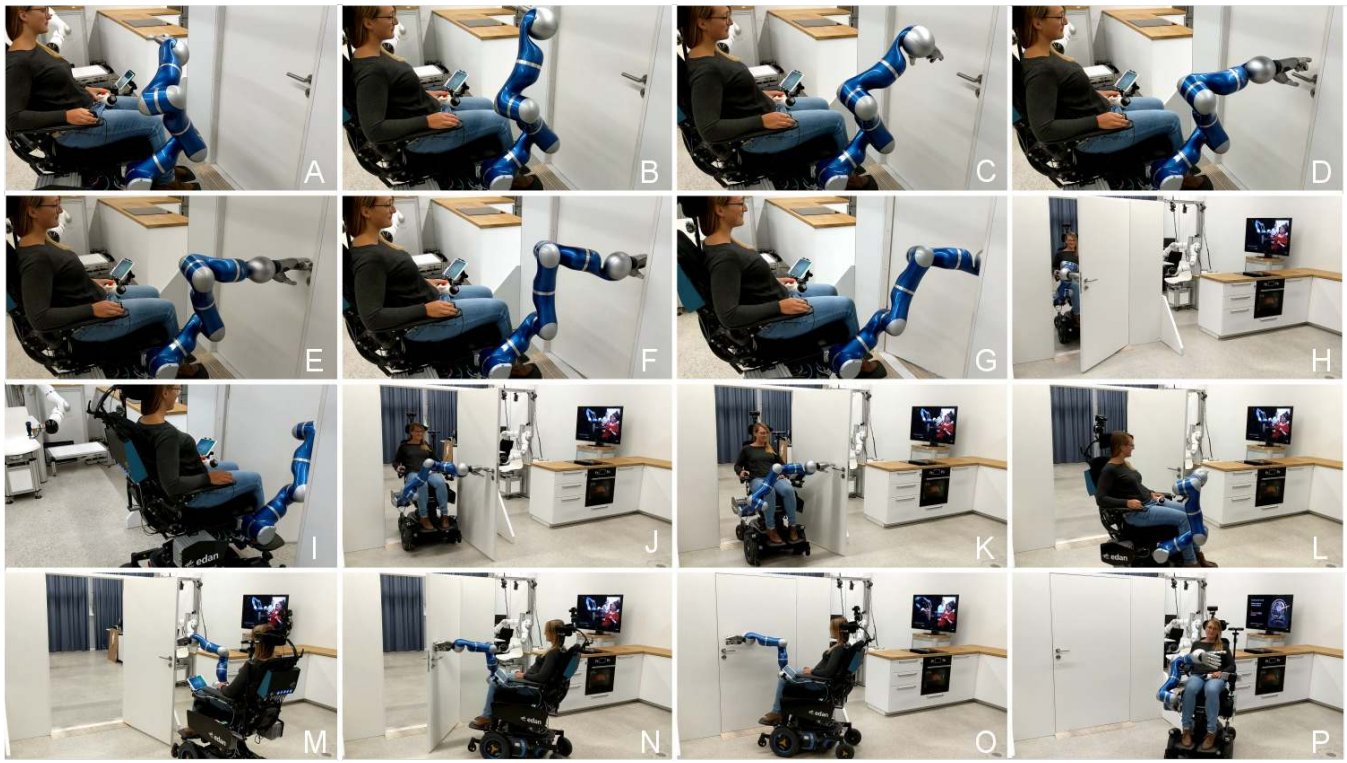

Fig. 9: Photo series of the different phases of the task: approach (A), alignment to the door (B), open the door (C-H), drive through (I-L) and finally close the door (M-O), executed by means of shared-control and whole-body control on the EDAN system (please note that this is a demonstration with a non-disabled user).

backward motion only, which is commanded from the WBC to ensure arm reachability. At the same time, the angular velocity is commanded from an absolute orientation controller which is active to keep the rotation of the wheelchair fixed, see Fig. 8c. Enforcing this initial orientation (being normal to the door) is essential to avoid collisions when passing through, especially because the width of the door frame and the system is 95 cm and 84 cm, respectively. An additional safety threshold for protecting the user is set where the WBC deactivates the wheelchair motion when the end-effector gets too close to the user. This can be seen in Fig. 8 as it modifies the forward velocity command when the threshold is exceeded. The positions of the wheelchair and the end-effector are depicted in Fig. 7.

3) Door closing: Snapshots of closing the door are displayed in Fig. 9M-O, where the user freely commands the hand motion while the WBC boundaries apply. Here, two DOF of the platform motion are commanded and coordinated through the WBC.

Fig. 7 is showing the robot hand and the wheelchair positions while opening and passing through the door, accordingly Fig. 8 is showing the WBC behavior and at which points of time the wheelchair motion is commanded. Footage of this task and additional capabilties of WBC is contained in the video attachment accompanying this manuscript.

D. Following Mode

To validate the following mode, a person interacts (e.g. pushes or pulls) with the robot hand, while the whole platform moves accordingly. This is demonstrated in the third part of the attached video[3]. The resulting actuation torques and generated velocity commands from this interaction are depicted in Fig. 10. In this mode the whole-body motion is active including the impedance controller (19), and the platform commands are computed according to the mapping of the interaction forces (24). The noisy raw signal of the estimated external forces can be used thanks to the admit-

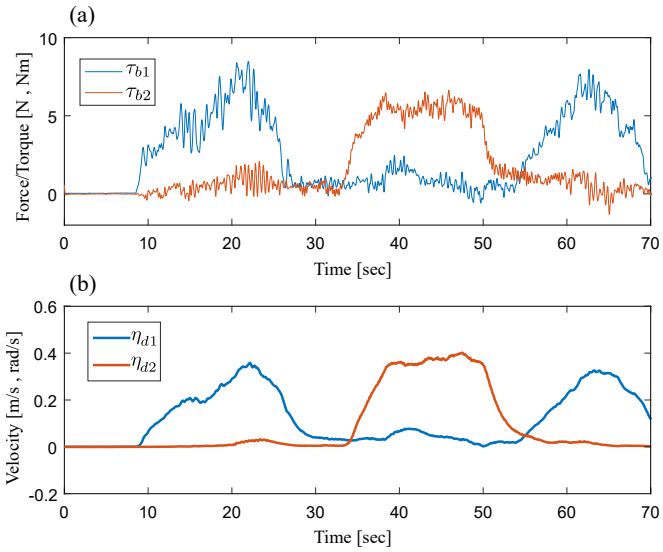

Fig. 10: Experimental results of the following mode. (a) shows the actuation forces of the mobile platform as a result of an interaction at the end-effector. In (b) the corresponding commanded velocities are shown.

[3]A high resolution video showing the WBC features is available at: https://youtu.be/78b39WsVFRI

tance interface (9), generating smooth commanded velocities due to the filtering effect. As shown in Fig. 10 the system can be manually maneuvered by direct interaction with the end-effector, without the need for an extra input device. Moreover, the physical mass and inertia can be shaped such that only a small interaction force is needed to accelerate and decelerate the complete system.

V. Discussion and conclusion

A framework for a whole-body control method applied to the assistive robotic system EDAN was presented. First, crucial components of the method, the odometry model and the velocity controller, were validated experimentally. The application of opening, going through and closing a door was then demonstrated to show the capabilities of the approach. This application shows how the user can benefit from whole-body control in combination with shared control for tasks which require a long range of motion. Without whole-body control, a sequential approach, alternating between control of the arm and the platform would be needed. Actually, the movement constraints arising from grasping the door handle would even prevent the user from moving the wheelchair in a sequential door opening approach, necessitating to release the handle before relocating the wheelchair. In comparison, our method allows the user to only control the end-effector with guidance from the shared control, while the wheelchair automatically moves accordingly, ensuring the completion of this task.

Future work targets the integration of new tasks, which require a large range of motion. Irrespective of the task, employing whole-body control in the EDAN scenario frees the user from planning for a proper wheelchair position when approaching an object, as reachability can be automatically restored during the manipulation. Furthermore, this approach could also be used to optimize manipulability of the arm, by moving the platform accordingly during a task. Finally, testing the complete system behavior by people with disabilities is one of the next research points.

References

[1] R. L. Bennett, "The evolution of the georgia warm springs foundation feeder," *Physical Therapy Review*, vol. 36, no. 11, 1956.

[2] G. Kramer, G. Römer, and H. Stuyt, "Design of a Dynamic Arm Support (DAS) for gravity compensation," 2007, pp. 1042–1048.

[3] V. Maheu, P. S. Archambault, J. Frappier, and F. Routhier, "Evaluation of the JACO robotic arm: Clinico-economic study for powered wheelchair users with upper-extremity disabilities," in *Rehabilitation Robotics (ICORR), 2011 IEEE International Conference on*. IEEE, 2011, pp. 1–5.

[4] W. Seamone and G. Schmeisser, "Early clinical evaluation of a robot arm/worktable system for spinal-cord-injured persons." *Journal of rehabilitation research and development*, vol. 22, no. 1, pp. 38–57, 1985.

[5] M. Topping, "An overview of the development of Handy 1, a rehabilitation robot to assist the severely disabled," *Journal of Intelligent & Robotic Systems*, vol. 34, no. 3, pp. 253–263, 2002.

[6] K. Corker, J. H. Lyman, and S. Sheredos, "A preliminary evaluation of remote medical manipulators," *Bull Prosthet Res*, vol. 16, no. 2, pp. 107–34, 1979.

[7] H. Kwee, J. Duimel, J. Smits, A. T. de Moed, J. van Woerden, L. van de Kolk, and J. Rosier, "The Manus wheelchair-borne manipulator: System review and first results," in *Proc. IARP Workshop on Domestic and Medical & Healthcare Robotics, Newcastle*, 1989.

[8] G. Romer, H. J. Stuyt, and A. Peters, "Cost-savings and economic benefits due to the assistive robotic manipulator (ARM)," in *Rehabilitation Robotics, 2005. ICORR 2005. 9th International Conference on*. IEEE, 2005, pp. 201–204.

[9] A. Hagengruber, D. Leidner, and J. Vogel, "EDAN: EMG-controlled daily assistant," in *Proceedings of the Companion of the 2017 ACM/IEEE International Conference on Human-Robot Interaction*. ACM, 2017, pp. 409–409.

[10] L. R. Hochberg, D. Bacher, B. Jarosiewicz, N. Y. Masse, J. D. Simeral, J. Vogel, S. Haddadin, J. Liu, S. S. Cash, P. van der Smagt *et al.*, "Reach and grasp by people with tetraplegia using a neurally controlled robotic arm," *Nature*, vol. 485, no. 7398, p. 372, 2012.

[11] J. Vogel and A. Hagengruber, "An sEMG-based Interface to give People with Severe Muscular Atrophy control over Assistive Devices," in *2018 40th Annual International Conference of the IEEE Engineering in Medicine and Biology Society (EMBC)*. IEEE, 2018, pp. 2136–2141.

[12] J. Vogel, K. Hertkorn, R. U. Menon, and M. A. Roa, "Flexible, semi-autonomous grasping for assistive robotics," in *2016 IEEE International Conference on Robotics and Automation (ICRA)*. IEEE, 2016, pp. 4872–4879.

[13] Y. Yamamoto and X. Yun, "Coordinating locomotion and manipulation of a mobile manipulator," in *[1992] Proceedings of the 31st IEEE Conference on Decision and Control*. IEEE, 1992, pp. 2643–2648.

[14] O. Khatib, "Mobile manipulation: The robotic assistant," *Robotics and Autonomous Systems*, vol. 26, no. 2-3, pp. 175–183, 1999.

[15] A. Dietrich, T. Wimböck, and A. Albu-Schäffer, "Dynamic Whole-Body Mobile Manipulation with a Torque Controlled Humanoid Robot via Impedance Control Laws," in *Proc. of the 2011 IEEE/RSJ International Conference on Intelligent Robots and Systems*, September 2011, pp. 3199–3206.

[16] A. Dietrich, *Whole-Body Impedance Control of Wheeled Humanoid Robots*, ser. Springer Tracts in Advanced Robotics. Springer International Publishing, 2016, vol. 116.

[17] C. Ott, B. Bäuml, C. Borst, and G. Hirzinger, "Autonomous opening of a door with a mobile manipulator: A case study," *IFAC Proceedings Volumes*, vol. 40, no. 15, pp. 349–354, 2007.

[18] S. Chitta, B. Cohen, and M. Likhachev, "Planning for autonomous door opening with a mobile manipulator," in *2010 IEEE International Conference on Robotics and Automation*. IEEE, 2010, pp. 1799–1806.

[19] A. Hagengruber and J. Vogel, "Functional Tasks Performed by People with Severe Muscular Atrophy Using an sEMG Controlled Robotic Manipulator," in *2018 40th Annual International Conference of the IEEE Engineering in Medicine and Biology Society (EMBC)*. IEEE, 2018, pp. 1713–1718.

[20] B. Siciliano and O. Khatib, *Springer handbook of robotics*. Springer, 2016.

[21] G. Campion, G. Bastin, and B. D'Andréa-Novel, "Structural Properties and Classification of Kinematic and Dynamic Models of Wheeled Mobile Robots," *IEEE Transactions on Robotics and Automation*, vol. 12, no. 1, pp. 47–62, February 1996.

[22] M. Iskandar and S. Wolf, "Dynamic friction model with thermal and load dependency: modeling, compensation, and external force estimation," in *2019 IEEE International Conference on Robotics and Automation (ICRA)*. IEEE, 2019, pp. 7367–7373.

[23] S. Wolf and M. Iskandar, "Extending a dynamic friction model with nonlinear viscous and thermal dependency for a motor and harmonic drive gear," in *2018 IEEE International Conference on Robotics and Automation (ICRA)*. IEEE, 2018, pp. 783–790.

[24] A. Albu-Schäffer, C. Ott, and G. Hirzinger, "A Unified Passivity-based Control Framework for Position, Torque and Impedance Control of Flexible Joint Robots," *International Journal of Robotics Research*, vol. 27, no. 1, pp. 23–39, January 2007.

[25] A. Dietrich, C. Ott, and A. Albu-Schäffer, "An overview of null space projections for redundant, torque-controlled robots," *International Journal of Robotics Research*, vol. 34, no. 11, pp. 1385–1400, Sept. 2015.

[26] A. De Luca, A. Albu-Schäffer, S. Haddadin, and G. Hirzinger, "Collision detection and safe reaction with the DLR-III lightweight manipulator arm," in *Intelligent Robots and Systems, 2006 IEEE/RSJ International Conference on*. IEEE, 2006, pp. 1623–1630.

[27] T.-Y. Lin, P. Goyal, R. Girshick, K. He, and P. Dollár, "Focal loss for dense object detection," *IEEE transactions on pattern analysis and machine intelligence*, 2018.